Science of the Total Environment 701 (2020) 134919

Contents lists available at ScienceDirect

Science of the Total Environment

journal homepage: www.elsevier.com/locate/scitotenv

Limited Cu(II) binding to biochar DOM: Evidence from C K-edge NEXAFS and EEM-PARAFAC combined with two-dimensional correlation analysis

Jing Wei [a], Chen Tu [a], Guodong Yuan [b,*], Yongqiang Zhou [c], Hailong Wang [d,e], Jian Lu [a,*]

[a] CAS Key Laboratory of Coastal Environmental Processes and Ecological Remediation, Yantai Institute of Coastal Zone Research, Chinese Academy of Sciences, Yantai 264003, China
[b] School of Environmental and Chemical Engineering, Zhaoqing University, Zhaoqing 526061, China
[c] Stated Key Laboratory of Lake Science and Environment, Nanjing Institute of Geography and Limnology, Chinese Academy of Sciences, Nanjing 210008, China
[d] Biochar Engineering Technology Research Center of Guangdong Province, School of Environmental and Chemical Engineering, Foshan University, Foshan 528000, China
[e] Zhejiang Province Key Laboratory of Soil Contamination and Bioremediation, Zhejiang A&F University, Hangzhou 311300, China

HIGHLIGHTS

- NEXAFS and EEM were used to probe the capacity of biochar DOM to bind Cu(II).
- Pyrolysis temperature and DOM components determine the binding capacity.
- Humic components showed a higher Cu-binding capacity than protein component.
- The capacity of DOM to bind Cu(II) reduced with rising pyrolysis temperature.
- The DOM generally had low Cu(II) binding capacity.

GRAPHICAL ABSTRACT

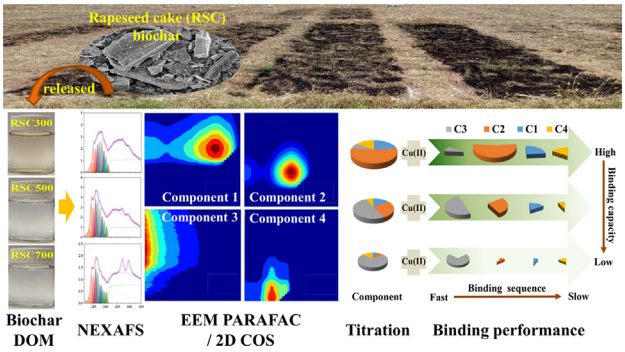

ARTICLE INFO

Article history:
Received 24 July 2019
Received in revised form 9 October 2019
Accepted 9 October 2019
Available online 2 November 2019

Editor: Daniel CW Tsang

Keywords:
Biochar
DOM
C K-edge NEXAFS
EEM-PARAFAC
2D-COS
Cu binding

ABSTRACT

Multiple spectroscopic technologies and chemometric analyses were combined to explore the compositional characteristics and Cu binding performance of biochar-derived dissolved organic matter (DOM). The DOM samples were extracted from biochars produced from lignocellulose-rich rapeseed cake (RSC) by pyrolysis at 300, 500, and 700 °C (i.e., RSC300, RSC500, RSC700). Fourier transform infrared spectroscopy (FTIR) and carbon K-edge near-edge X-ray absorption fine structure spectroscopy (NEXAFS) analyses were combined to elucidate the molecular-level C species in the DOM. With the increasing pyrolysis temperature, DOM aromaticity increased, whereas the proportion of metal complexing sites (e.g., carboxyl and phenolic groups) decreased. Fluorescence excitation-emission matrix (EEM) spectroscopy with parallel factor analysis (PARAFAC) indicated that biochar DOM, irrespective of pyrolysis temperature, was mostly composed of three types of humic-like components (C1–C3), and a small amount of a protein-like component (C4). As charring temperature increased, DOM concentrations decreased substantially, but the humic-like C3 with abundant aromatic structures became predominant. Fluorescence quenching experiment and two-dimensional correlation spectroscopy (2D-COS) analysis suggested that the preferential Cu(II) binding fractions of the DOM were the humic-like substances. Moreover, the quenching curve fitting results for individual components indicated that despite the Cu (II) binding affinity was slightly enhanced as the pyrolysis temperature increased, the binding capacities

* Corresponding authors.
E-mail addresses: yuanguodong@zqu.edu.cn (G. Yuan), jlu@yic.ac.cn (J. Lu).

https://doi.org/10.1016/j.scitotenv.2019.134919

of the four components decreased. In general, the DOM components from RSC biochar exhibited limited Cu(II) binding capacities (2.18–17.7 μmol L^{-1}). Results from this study improved understanding of the mechanisms by which biochar DOM interacts with Cu, and provided tools for fast screening of biochars to reduce their environmental risks.

1. Introduction

Biochar, a carbon-rich material produced from the pyrolysis of biomass, has been intensively investigated for potential use as a soil amendment for agronomic (El-Naggar et al., 2019; Li et al., 2019; Wu et al., 2019) and environmental benefits (Lu et al., 2017; Sun et al., 2019; Xia et al., 2019). Biochar amendment is known to introduce dissolved organic matter (DOM) into soil solution, thus changed the content and composition of soil DOM, further affecting the soil microbial activity and trace metal immobilization (Beesley et al., 2010; Yang et al., 2019).

DOM in the biochar actually was consisted of both original components in the feedstock and pyrolysis products, such as humic- and protein-like substances, which have been identified by a variety of spectroscopic and mass spectrometric techniques (Li et al., 2017; Qu et al., 2016; Smith et al., 2016; Uchimiya et al., 2013). Numerous studies have indicated that the chemical compositions of DOM varied greatly from the feedstocks and pyrolysis temperatures of biochar, as well as the extraction protocols (Lee et al., 2018; Wei et al., 2019a; Wu et al., 2018). Among these parameters, pyrolysis temperature was usually a vital determinant of the DOM characteristics (Liu et al., 2019; Wu et al., 2019). Rajapaksha et al. (2019) observed that the increased pyrolysis temperature could increase the relative proportion of humic-like substances in the biochar DOM. Similarly, Wu et al. (2019) found that the proportion of humic-like substances clearly increased with the increasing pyrolysis temperature, while the proportion of fulvic-like substances exhibited an opposite trend. Recently, advanced synchrotron-based spectroscopic techniques, such as carbon (C) K-edge near-edge X-ray absorption fine structure spectroscopy (NEXAFS), have been used to further probe the in-situ chemical state and functional groups of biochars (Singh et al., 2014; Wei et al., 2019b) and their released DOM (Wei et al., 2019a). This highly sensitive and non-destructive technique is particularly suitable for the analysis of DOM extracted from high-temperature biochar because of the scarcity of the DOM. Wei et al. (2019a) investigated the molecular structure of DOM from halophyte derived biochars by the C K-edge NEXAFS, and the functional groups identified included hydroxyl, carboxyl, phenyl, ether, amine, and alkyl. Further, the carboxyl group gradually decreased with the increasing pyrolysis temperature.

Given its abundant reactive functional groups, biochar-DOM is speculated to have strong interactions with metal contaminants (Li et al., 2018; Li et al., 2017; Uchimiya et al., 2010). A few studies have described that natural DOM may combine contaminants and facilitate their transport with the development of advanced analysis methods. For example, fluorescence excitation-emission matrix (EEM) spectroscopy coupled with parallel factor analysis (PARAFAC) has been recognized as a fast and in-situ tool for characterizing the metal-binding performance of DOM from compost, soil, and freshwater (Hu et al., 2017; Wei et al., 2015). Moreover, the affinities and capacities of individual PARAFAC components to bind heavy metals can be derived via fitting fluorescence quenching models (e.g., the Ryan and Weber model (Luster et al., 1996)). Similarly, two-dimensional correlation spectroscopy (2D-COS) analysis can be used to resolve the overlapped fluorescence spectroscopy and identify the heterogeneous distribution of metal-binding sites (Hur and Lee, 2014; Noda and Ozaki, 2004). More importantly, it can be used to obtain information on the sequence of the response of the DOM components to the heavy metal addition (Hu et al., 2017; Xu et al., 2013). A combination of these spectroscopic and chemometric methods has been proved powerful in probing the heavy metal binding mechanisms. By using EEM-PARAFAC, Hu et al. (2017) found the impoundment could increase the Cu binding affinities of humic-like components of DOM in lake water while decreasing those of the protein-like components. Meanwhile, 2D-COS analysis indicated that the prior Cu binding sites was the humic-like components in early impoundment stage, but switched to the protein-like components.

Despite numerous studies on the interactions of natural DOM with metal ions, only a few have focused on the biochar-derived DOM. For instance, Kim et al. (2018) investigated the effects of biochar DOM on the mobility of arsenic (As) in soil and concluded that biochar produced at low temperature (300 °C) could release a large amount of DOM and enhance the reductive dissolution of Fe and the mobilization of As. Regarding the intrinsic interaction between biochar-derived DOM and heavy metals, Huang et al. (2019) compared the Cu and Cd binding behavior of different DOM components derived from rice straw biochar and found that the metal-binding sequence was highly related to both heavy metal elements and DOM components. However, studies regarding the temperature-dependent metal-binding behavior of biochar-derived DOM and the relations to their molecular structures under different pyrolysis temperatures are still limited. Thus, further researches are needed to fill the gap in predicting the bioavailability and mobility of heavy metals in the biochar-soil systems, with the integrative application of advanced spectroscopy and chromatography techniques.

In this study, rapeseed cake (RSC) was chosen as the biochar feedstock. As China is the second in the world in terms of the rapeseed cultivation area (Lomascolo et al., 2012), RSC is a readily available biowaste. Meanwhile, Cu(II) was selected as the target metal element because it is a common contaminant in agricultural soils of China (MEP and MLR, 2014) and high toxicity to soil microbial community and plant flora (Tu et al., 2018). Pyrolysis temperature (300, 500, and 700 °C) was evaluated for its effects on the composition and Cu(II) binding performance of biochar-derived DOM. Fourier transform infrared (FTIR) spectroscopy, C K-edge NEXAFS, and EEM-PARAFAC were employed to characterize biochar DOM from varying pyrolysis temperatures. Fluorescence quenching experiment combined with 2D-COS and PARAFAC analyses was used to quantitatively evaluate the Cu(II) binding affinities and capacities of DOM components. The obtained results would help understand the mechanisms of DOM-Cu interactions in soil and assess the risk from biochar application for immobilizing Cu in soil environment.

2. Materials and methods

2.1. Extraction and pretreatment of biochar-derived DOM

Raw rapeseed cake was obtained from a vegetable oil processing plant in Nanjing, Jiangsu Province, China. After oven-drying at 80 °C for 48 h, the RSC pieces were ground and mixed uniformly. The powdered feedstock was pyrolyzed under purified N_2 purging,

with a heating rate of 5 °C/min in a tube furnace. After the temperature reached 300, 500, or 700 °C the pyrolysis continued for 6 h before cooling to room temperature, resulting in a biochar yield of 36.4%, 31.5%, and 28.7%, respectively.

The produced biochars were ground and sieved to <0.25 mm (60 mesh). This size fraction was chosen to represent small biochar particles that showed a greater potential for DOM releasing once applied to soil (Liu et al., 2019). The DOM was obtained by shaking the suspension of biochar with Milli-Q water at a ratio of 1:100 m/v on an oscillator for 48 h at 25 °C and then vacuum-filtering through 0.45 μm polytetrafluoroethylene membranes. The DOM samples obtained were labeled RSC300, RSC500, and RSC700, where the suffix number indicated the pyrolysis temperature. DOM samples were stored in a brown glass bottle at 4 °C and analyzed within one week for pH by using a pH meter (Mettler Toledo, Switzerland), alkali and alkaline earth metal concentrations by a PerkinElmer ELAN DRC II ICP-MS (PerkinElmer, USA), dissolved organic carbon (DOC) by a Shimadzu TOC-VCPH TOC analyzer (Shimadzu, Japan), and fluorescence as detailed in section 2.4. A subsample of each was freeze-dried for FTIR and C K-edge NEXAFS measurement.

2.2. FTIR and C K-edge NEXAFS analyses of biochar-derived DOM

Samples for FTIR measurement were prepared by homogeneously mixing freeze-dried DOM with KBr (IR grade) at a ratio of 1:100 (m/m) to press into KBr wafers. FTIR spectra, as shown in the supplementary information (SI, Fig. S1), were recorded using a FT/IR-4100 spectrophotometer (Jasco, Japan) between 400 and 4000 cm^{-1} at a resolution of 4 cm^{-1}.

The C K-edge NEXAFS measurement was conducted at the soft X-ray spectromicroscopy beamline (BL08U1A) of the Shanghai Synchrotron Radiation Facility, China. The preparation of specimens was described elsewhere (Wei et al., 2019b). Briefly, a freeze-dried DOM sample was dispersed uniformly with Milli-Q water and deposited onto a gold-sprayed silicon wafer to form thin films. Each air-dried film was measured for C K-edge NEXAFS data at total electron yield mode from 280 to 310 eV with an increment of 0.1 eV. For the semi-quantitative assessment of C species abundance in biochar DOM, the NEXAFS spectra were deconvoluted by the PeakFit v4.12 software (SeaSolve) according to the method of Wei et al. (2019b). Peak energy ranges and assignments for carbon functional group are summarized in SI Table S1.

2.3. Cu(II) titration experiment

Copper stock solutions (0.1 and 1.0 mol/L) were prepared using $Cu(NO_3)_2$ (Aladdin, Shanghai, China). DOM solutions were diluted, for eliminating the fluorescence inner-filter effect, to give DOC concentrations of 12.3, 5.7, and 4.6 mg/L for RSC300, RSC500, and RSC700, respectively. Meanwhile, the inherent alkali and alkaline earth metal concentrations were diluted so that they would have no interference with the fluorescence spectroscopy. Quenching titrations were conducted by adding Cu stock solutions to 25 mL of the DOM solutions in 40 mL brown vials. The Cu(II) concentrations in the final solutions ranged from 0 to 60 μmol/L (i.e., 0, 4, 6, 12.5, 20, 30, 40, and 60 μmol/L). This concentration range was set to mimic Cu concentrations in natural conditions. A higher Cu concentration might lead to DOM aggregation (Wei et al., 2015). Each treatment was carried out in triplicate. The initial pH of RSC300, RSC500, and RSC700 were 7.14, 8.33, and 7.99, respectively. To maintain constant pH and prevent Cu precipitation, all titrated solutions were adjusted to pH = 6.00 ± 0.05 using HNO_3 or NaOH (0.1 and 1.0 mol/L). All titrated solutions were then shaken at 25 °C for 24 h to ensure complexation equilibrium.

2.4. Fluorescence analysis

The fluorescence EEMs of biochar DOM samples and Milli-Q water blank were measured using an Aqualog spectrometer (HORIBA, Japan) at 3D mode, with an excitation wavelength (Ex) range set from 200 to 450 nm (5 nm intervals) and an emission wavelength (Em) range set from 245 to 825 nm (1 nm intervals). Raman scatter and Rayleigh scattering effects were removed by Aqualog software package. Subsequently, the EEMs were normalized by the integrated area of the blank water Raman peak (Ex = 350 nm) and presented in Raman units (R.U.) (Lawaetz and Stedmon, 2009). Representative EEM spectra of the DOM from RSC biochar are shown in the SI, Fig. S2.

PARAFAC modeling was applied to identify the fluorescent components of the biochar DOM, conducted in MATLAB R2014a (MathWorks) with the DOMFluor toolbox (www.models.life.ku.dk) (Zhou et al., 2017). The PARAFAC was computed using 2–7 components models for the biochar DOM dataset, which contained a total of 72 EEMs from the titration experiment. The optimal components number for the biochar DOM dataset was determined through split half analysis, residual analysis, and visual inspection. Fig. S3 in SI exhibits the EEM spectral loadings of PARAFAC components modeled with the halves of the dataset and on the whole dataset of RSC biochar DOM.

Furthermore, fluorescence spectroscopy coupling with 2D-COS analysis was employed to obtain the sequential orders of Cu binding with the biochar DOM compositions. Two types of the maps, synchronous and asynchronous 2D-COS maps, were generated using the region of a constant Ex = 255 nm with Em ranging from 282 to 655 nm in the EEM matrixes for RSC biochar DOM with Cu addition. The changes in the selected region of fluorescence spectra for the Cu titration DOM samples are presented in SI Fig. S4. The 2D-COS analysis was performed according to the method of Noda and Ozaki (2004), using the MIDAS 2010 toolbox released by the University of Saskatchewan, Canada (Zhou et al., 2017). Besides, the modified Ryan-Weber model was used to determine the Cu(II) binding capacity and affinity of different components of the biochar DOM. More detailed information about the model can be found in SI.

2.5. Statistical analysis

Results were reported as averages of the triplicate analyses. Significant differences were analyzed using one-way ANOVA with Duncan's multiple range test at $p < 0.05$ using the SPSS 19.0 software package (IBM, USA).

3. Results and discussion

3.1. DOM content in biochars as affected by pyrolysis temperature and feedstock

With a rise in pyrolysis temperature, DOM released from RSC biochars quickly decreased from 2.73 ± 0.19 g C/kg in RSC300 to 0.19 ± 0.001 in RSC500 and 0.13 ± 0.02 g C/kg in RSC700 (Table 1). This trend was also observed for biochars produced from other lignocellulose-rich feedstocks, such as Jerusalem artichoke stalks (Wei et al., 2019a), rice straws (Xiao et al., 2014), and wetland plant litters (Wu et al., 2019). DOM content in biochar was primarily affected by pyrolysis temperature and feedstock. During the biomass pyrolysis, some condensable volatiles (e.g., bio-oil-like substances) could be captured by porous biochar, and later released as DOM (Cole et al., 2012). With an increase in pyrolysis temperature, the condensable volatiles could be further cracked or re-polymerized into biochar structure via secondary reactions

Table 1
Concentrations of dissolved organic carbon (DOC), water-extractable alkali and alkaline earth metals in RSC biochars.

	Unit	RSC300	RSC500	RSC700
Organic carbon contents				
DOC	mg/g	2.73 ± 0.19[a]	0.19 ± 0.001[b]	0.13 ± 0.02[b]
Total solute	mg/g	25.8 ± 1.4[a]	15.8 ± 2.0[b]	12.2 ± 1.4[b]
DOC in total solute	%	10.6	1.2	1.1
Mineral metal contents				
Na	mg/kg	90 ± 2[a]	68 ± 4[b]	53 ± 2[c]
K	mg/kg	380 ± 10[a]	302 ± 2[b]	219 ± 1[c]
Ca	mg/kg	2189 ± 80[a]	287 ± 11[b]	270 ± 12[b]
Mg	mg/kg	103 ± 1[a]	50 ± 3[b]	40 ± 1[c]

Data are presented as the average value ± standard deviation. Different superscripted letters indicate significant differences among DOM from biochars produced at different temperatures.

such as aromatization and condensation (Sullivan and Ball, 2012; Liu et al., 2019), thus resulting in a lower DOM content of the biochar produced at higher pyrolysis temperature.

On the other hand, DOM in biochar consisted of some original components (such as lipids) in the feedstock, which could also affect the content of biochar DOM. Being produced under the same pyrolysis conditions, biochar made from Jerusalem artichoke stalks (JAS) (Wei et al., 2019a) had much higher DOM contents than those of RSC biochars. For example, the 300 °C JAS biochar had the DOM content up to 23.00 g C/kg. JAS was rich in Ca, and it is known to inhibit the decomposition of cellulose by increasing thermal stability, thereby promoting char formation (Thyrel et al., 2016) and resulting in high yields of JAS biochar (from 45.2% to 30.2%) and a large amount of DOM (Wei et al., 2019a). In contrast, Na and K in feedstock may act as catalysts in the pyrolysis of lignocelluloses (Kleen and Gellerstedt, 1995), producing a much lower DOM content in RSC biochars. Thus, it could be expected that the RSC biochars would have a low DOM leaching risk if applied to soils.

RSC300 biochar released more alkali and alkaline earth metals than RSC500 and RSC700 (Table 1). This decrease in the concentration of water-extractable metals with rising pyrolysis temperature was in agreement with Kloss et al. (2012). It might be attributed to the formation of insoluble minerals (e.g., calcite, maghemite) together with some clay minerals such as anorthite and muscovite at high temperatures (Xu et al., 2016). Our investigations indicate that RSC biochars, especially those prepared at high temperatures (≥500 °C), can release limited amounts of dissolved organic carbon and metallic species into water under natural conditions.

3.2. Carbon speciation of biochar DOM

To better understand the pyrolysis temperature-induced changes in molecular compositions of biochar DOM, C K-edge NEXAFS and FTIR were combined to identify the carbon speciation of biochar DOM. Functional groups that are common to bulk biochars and natural DOM, including hydroxyl, carboxyl, phenyl, ether, amine, and alkyl (Abdulla et al., 2010; Wei et al., 2019b), have also been identified in DOM from biochars, suggesting that the nature of the carbon-containing moieties may be similar. The FTIR spectra of RSC biochar DOM exhibited the COO^- bands (asymmetric stretching at 1590–1635 cm^{-1}, symmetric stretching around 1400 cm^{-1}) and heat-resistant aliphatic CH_x bands (2980–2850 cm^{-1}), regardless of charring temperature (SI Fig. S1). As pyrolysis temperature increased, the broad bands assigned to hydrogen-bonded O—H stretching (3600–3200 cm^{-1}) weakened, mainly resulting from dehydroxylation. In the spectra of RSC500 and RSC700, the absorbances of aromatic C—H stretching (870–690 cm^{-1}) were significantly higher than those in the spectrum of RSC300.

Carbon K-edge NEXAFS spectra of each RSC biochar DOM are displayed in Fig. 1. For the semiquantitative comparison of C species present in the biochar DOM, the relative proportions of the primary C species were derived by spectra fitting of the corresponding peaks (Table 2). Combining our previous characterization of JAS biochar DOM, we confirmed that biochar DOM had similarity in organic C speciation with the bulk biochars (Singh et al., 2014; Wei et al., 2019a,b) and soil organic substances (Luo et al., 2017; Schafer et al., 2005), but varied in abundances of C species. The relative proportions of C species in the biochar DOM were greatly influenced by charring temperature. As illustrated in Fig. 1, the peaks of carboxyl-C (1s-π* transitions of carboxyl C═O) and aliphatic-C (1s-3p/σ* transition of aliphatic C—H) decreased with rising pyrolysis temperature, so were their proportions (Table 2). It has been found that 500 °C was a crucial temperature for the formation or decomposition of carboxyl groups. At temperature ≤500 °C, carboxyl groups were formed by hydroxyls oxidation, while at temperature >500 °C, they mainly decomposed via dehydrogenation and dihydroxylation (Harvey et al., 2012). Here, the concomitant increase of ketonic-C and carbonyl-C (1s-π* transition of ketonic C═O and carbonyl C═O) at ≥500 °C provided indirect evidence for carboxyl-C decomposition. Similarly, the peaks of quinonic-C and aromatic-C became more appreciable at 500 and 700 °C. Calculated as the ratio of total aromatic-C to carboxyl-C, the aromaticity of the biochar DOM, therefore, increased from

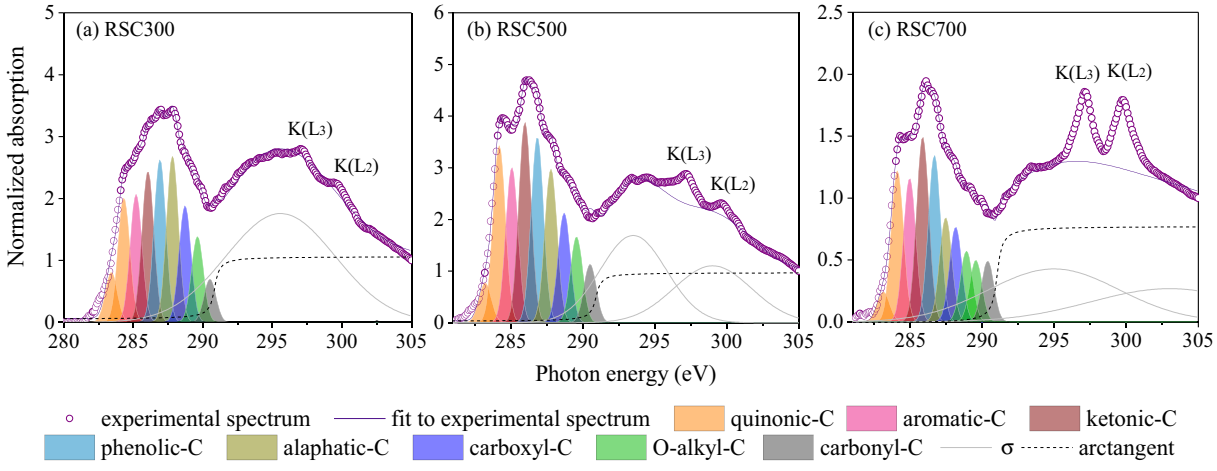

Fig. 1. Carbon K-edge NEXAFS spectra of DOM from RSC biochars produced at 300 (a), 500 (b), and 700 °C (c). Speciation of spectra deconvolution shows the main 1s-π* and 1s-3p/σ* transitions, σ* transitions, and arctangent step functions. Two adsorption peaks at 297 and 299 eV are attributed to potassium (K) L_3 and L_2 edges, respectively.

Table 2
Aromaticity and organic C species proportions (%) of biochar DOM identified by C K-edge NEXAFS spectra.

	RSC300	RSC500	RSC700
Aromaticity*	2.59	3.39	3.42
C species (eV)			
Quinonic-C (283.5–284.3)	17.0	18.6	16.9
Aromatic-C (284.8–285.3)	12.5	13.3	13.4
Ketonic-C (285.7–286.2)	14.7	17.2	17.3
Phenolic-C (286.6–287.1)	15.8	15.9	15.6
Aliphatic-C (287.5–287.9)	16.2	13.2	9.8
Carboxyl-C (288.2–288.6)	11.3	9.4	8.9
O-alkyl-C (288.8–289.5)	8.3	7.4	12.4
Carbonyl-C (290.0–290.5)	4.2	5.0	5.7

* Aromaticity = total aromatic-C/carboxyl-C; and total aromatic-C = quinonic-C + aromatic-C.

2.59 to 3.42 with rising pyrolysis temperature. This phenomenon was in line with an increase in the aromaticity of bulk biochar as the pyrolysis temperature raised (Awad et al., 2018; Wei et al., 2019b). Several studies have demonstrated that some quinonic and phenolic moieties in biochar DOM, regardless of charring temperatures, could function as electron shuttles (i.e., donate or accept electrons), thus regulating the biogeochemical redox reaction of heavy metals and nutrient elements in soil (Chen et al., 2018; Dong et al., 2014). Moreover, considering the decreased proportion of aliphatic-C, the DOM from high-temperature biochars was expected to have higher chemical recalcitrance than those from low-temperature biochars (Kleber et al., 2011).

3.3. PARAFAC components of biochar DOM

Four fluorescent components were identified in DOM from RCS biochars by PARAFAC analysis. Based on previous PARAFAC analysis of biochar DOM (Li et al., 2017; Uchimiya et al., 2013; Wei et al., 2019a) and natural DOM samples (Hu et al., 2017; Ishii and Boyer, 2012), we have assigned the components to three humic-like substances (C1, C2, and C3) and a protein-like (C4) substance. As shown in Fig. 2, C1 showed two Ex peaks: one below 230 nm and the other at 370 nm, corresponding to a single Em peak at 440 nm. These features are similar to those of typical terrestrial humic-like fluorophores (Wei et al., 2015; Zhou et al., 2017). C2 displayed a major Ex peak at 325 nm with a single Em peak at 380 nm. The Ex/Em peaks of this component were similar to those of a biologically degraded humic-like component (Fellman et al., 2010; Uchimiya et al., 2013). C3 had a single Ex peak below 230 nm with a broad Ex peak centered between 425 and 475 nm, similar to humic-like components associated with high aromaticity (Fellman et al., 2010; Hu et al., 2017). C4 had a distinct Ex_{max} at 280 nm and Em_{max} at 320 nm, mainly due to tyrosine-like substance (Zhou et al., 2017). This aromatic protein-like fraction was usually detected in DOM from biochars derived from lignin-rich feedstocks (Uchimiya et al., 2013).

As shown in Fig. 3a, the fluorescence intensities (R. U. unit per mg/L TOC) of humic C1 and C2 components declined as the charring temperature increases, indicating that C1 and C2 components were consumed during the pyrolysis process. Conversely, the humic C3 component exhibited a substantial increase in fluorescence intensity when the charring temperature was raised from 300 to 500 °C, and it became the predominant component at ≥500 °C (Fig. 3b). This trend is consistent with the work by Uchimiya et al. (2013), where a similar humic-like component of pecan shell-derived biochar DOC increased with charring temperature. A longer emission wavelength indicates more condensed, conjugated, and aromatic structures (Lichtman and Conchello, 2005). Combined FTIR and C NEXAFS results indicate that the C3

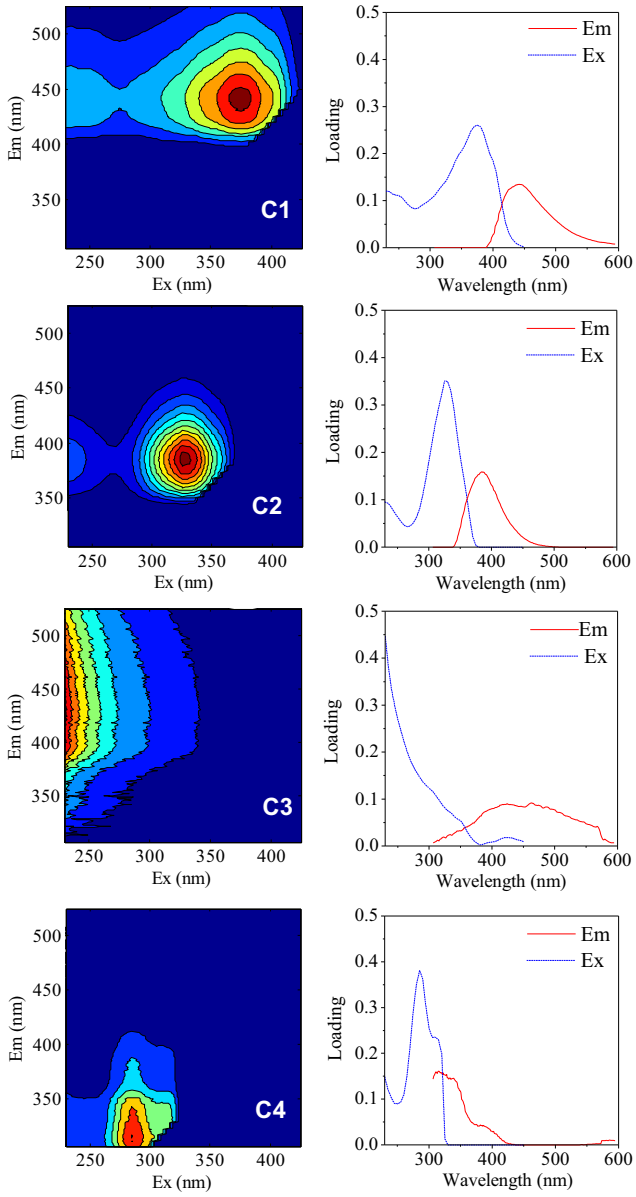

Fig. 2. The EEM contours of four PARAFAC components identified from RSC biochar DOM. C1, C2, and C3 refer to three humic-like components, and C4 refers to the protein-like component, respectively.

component is the major contributor to the aromaticity of DOM from high-temperature biochars. Indeed, the high level of C3 at high temperatures may largely be attributed to the chemical dehydroxylation, decarboxylation, and aromatization of biomass feedstock during the charring process. Finally, the fluorescence intensities of protein-like C4 dropped sharply from 300 to 500 °C, and further decreased slightly from 500 to 700 °C. These thermal-resistant protein-like substances were thought to come from the decomposition of lignin over a wide temperature range of 160–900 °C (Uchimiya et al., 2013; Yang et al., 2007).

The fluorescent feature of individual biochar DOM components strongly influences its photodegradation potential, and further its environmental behavior. Specifically, the primary and secondary fluorescent Ex/Em peaks of the humic-like C1 indicate that this component can absorb UVA and UVC light. Giving that UVC light is entirely absorbed by the ozone layer in the atmosphere, and the UV light that passes through the atmosphere remains about 94% UVA with UVB making up the rest (Diffey, 2002), the C1 is

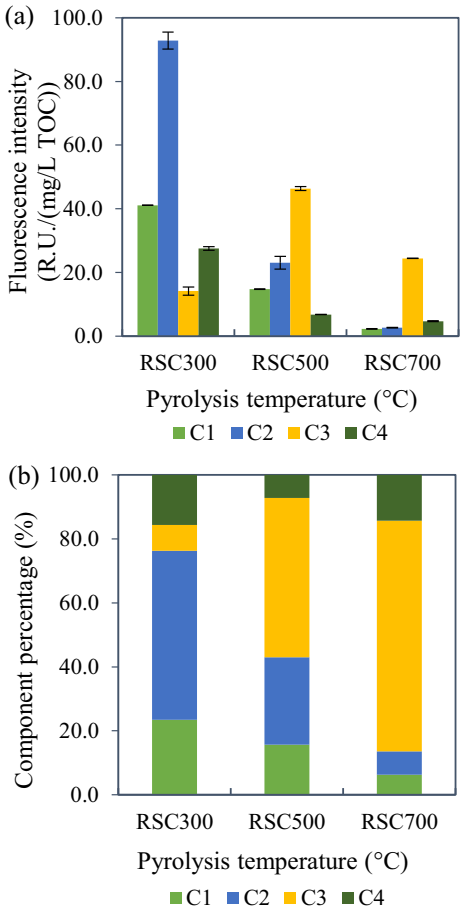

Fig. 3. The corresponding fluorescence intensities (a) and relative abundances (b) of four PARAFAC-derived components. C1, C2, and C3 refer to three humic-like components, and C4 refers to the protein-like component, respectively.

expected to be susceptible to UVA-induced photodegradation. By analogy, the humic-like C2 is likely to be photodegradable by UVA, although not as much as the C1 component because the Ex peak is partly blue-shifted to the UVB region (Ishii and Boyer, 2012; Qi et al., 2018). The humic-like C3 has a single Ex/Em peak and absorbs lights primarily in the UVC region. Recent work has found a similar component in surface water DOM undergone only a slight extent of photodegradation under solar irradiation (Wu et al., 2018). By analogy, C3 is expected to be relatively photo resistant in the terrestrial environment. Regarding the photodegradation behavior of protein-like component in natural DOM, conflicting findings were observed. Qi et al. (2018) reported that solar irradiation could increase the fluorescence intensity of protein-like DOM in coastal groundwater due to the photochemical synthesis process, whereas Wu et al. (2018) concluded that the aromatic proteins were easily photodegraded. Further studies are required to clarify the intricate photochemical features of biochar DOM and the potential environmental impacts.

Together with the relative abundance of the four components in biochar DOM (Fig. 3), the DOM from low-temperature biochar would be prone to photodegradation because of the high proportion of photodegradable C1 and C2. On the other hand, the DOM from biochar obtained at high pyrolysis temperature would be less susceptible to photodegradation, as indicated by the increased abundance of C3 with rising pyrolysis temperature. In combination with the results from C K-edge NEXAFS spectra, the temperature-dependent DOM compositions suggest that DOM from high-temperature biochar is more environmentally recalcitrant.

3.4. Binding features of biochar DOM with Cu(II)

The step addition of Cu(II) led to a gradual decrease in total fluorescent absorbance. Specifically, these decreased trends in the selected region of a constant Ex = 255 nm with Em ranging from 282 to 655 nm in the EEM matrixes are presented in SI Fig. S4. A similar phenomenon was also observed in the interaction between Cu and DOM from freshwater (Hu et al., 2017). The quenching effect was attributed to the donation of electrons from DOM compositions to Cu^{2+} (Lakowicz, 2006).

As shown in Fig. 4a–c, regardless of the DOM from biochars produced at different temperatures, all the synchronous maps displayed one positive autopeak (435 nm) along the diagonal line, indicating that the fluorescent intensities of all apparent compositions of biochar DOM decreased with increasing Cu concentration. Moreover, the extent of fluorescence reduction at Em wavelength 435 nm (i.e. humic-like C3) was most prominent. The RSC300 asynchronous map (Fig. 4d) exhibited two positive regions (350–380, 440–470; 405–425, 440–470), and three negative regions (290–320, 360–520), (375–400, 405–425), and (440–460, 490–510) above the diagonal line. Similarly, two positive regions (320–350, 440–470) and (405–425, 440–470), and two negative regions (285–310, 400–490) and (365–390, 410–435), which somewhat shifted from those identified from the RSC300 asynchronous map, were also observed in the RSC500 and RSC700 asynchronous maps. It is noticed that in Fig. 4e and f, the regions regarding of humic-like C1, C2, and protein-like C4, such as +(320–350, 440–470) and −(290–320, 360–520), remarkably weakened. This could be attributed to the sharp decreases in absorbances of these three components with the increasing temperature. Therefore, according to the sequential order rules (Noda and Ozaki, 2004), it could be concluded from the 2D-COS results that the Cu binding to the biochar DOM occurred in the order of humic-like C3 (Ex/Em: ~230/425 nm) > humic-like C2 (Ex/Em: ~325/380 nm) > humic-like C1 (Ex/Em: ~370/440 nm) > protein-like C4 (Ex/Em: ~280/320 nm). Similarly, Baken et al. (2011) and Chen et al. (2015) indicated that humic-like substances had a faster response than protein-like substances because of the higher aromaticity of the former.

Fig. 5 explicitly shows the effects of Cu(II) titration on the fluorescence absorbance of PARAFAC components (C1–C4) in biochar DOM. Here, Cu titration resulted in fluorescence quenching for all four components, and their quenching curves had similar trends to those of the fluorescent component identified in DOM from JAS biochar (Wei et al., 2019a). Of note, however, the amount of Cu-induced fluorescence quenching varied among the different components and among DOM from different biochars. These results reflected that the complexation characteristics between Cu(II) and each component of biochar DOM depended on the charring temperature and the precursor of the biochar.

As listed in Table 3, the binding capacities (C_L) of four components followed the sequence of C3 > C2 > C1 > C4, which were consistent with the 2D-COS results. Generally, humic-like component had a larger binding capacity of Cu than the protein-lick component. These results illuminated that humic-like substances in biochar DOM played the dominant role in binding heavy metals. Carboxyl and phenolic groups in DOM usually serve as complexing sites for metal cations. According to the Henderson-Hasselbalch equation, the ionization constant (pKa) is 3.0 for carboxyl groups and 10.0 for phenolic groups (Meng et al., 2017), implying that the carboxyl groups would be almost entirely ionized under the experimental conditions (pH = 6.00 ± 0.05), whereas phenolic groups would be little ionized. Thus, carboxyl groups would play the dominant role in Cu complexation. The NEXAFS results proved the reduction in carboxyl content of biochar DOM, which indicated a decrease in available complexing ligands. The complexation

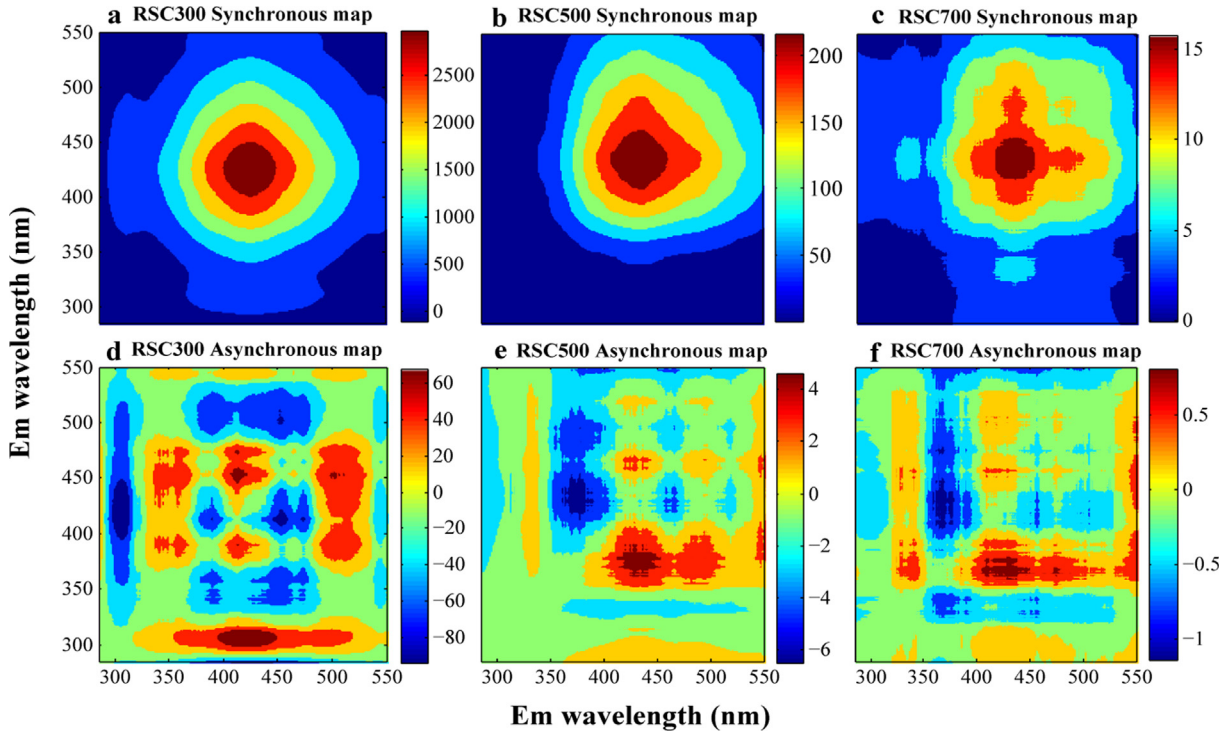

Fig. 4. Synchronous and asynchronous 2D correlation maps for RSC biochar DOM with Cu(II) addition.

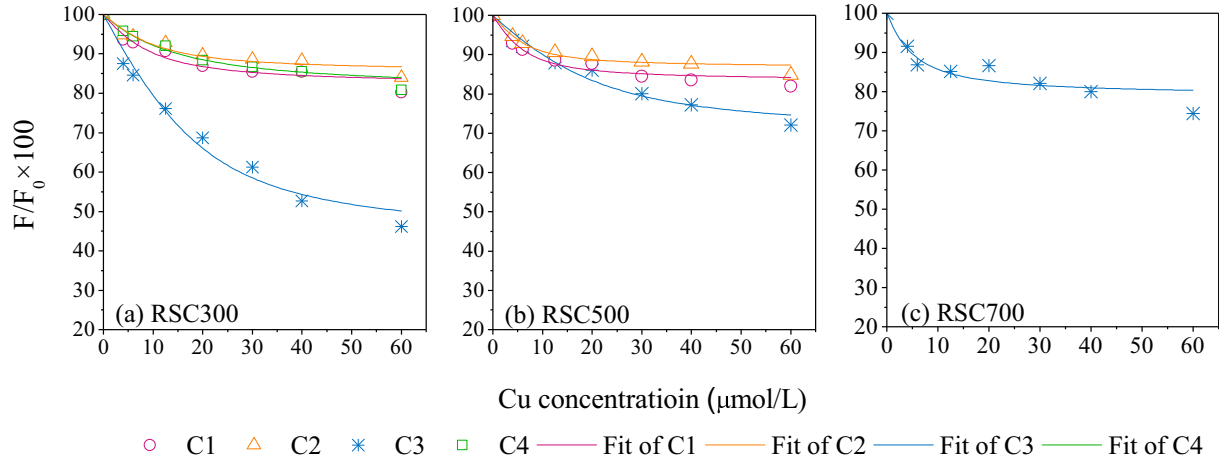

Fig. 5. The fluorescence quenching curves of the PARAFAC-derived components with Cu(II), presented as percent changes from initial levels ($F/F_0 \times 100$, where F and F_0 are the fluorescence intensity with and without Cu(II), respectively).

Table 3
Binding parameters of parallel factor analysis derived components with Cu(II) as determined by modified Ryan and Weber Model.

Biochar released DOM	PARAFAC components	log K_M	C_L (μmol L^{-1})	R^2
RSC300	C1	5.28	6.60	0.922
	C2	5.28	8.09	0.942
	C3	5.11	17.7	0.975
	C4	4.94	5.51	0.959
RSC500	C1	5.51	4.91	0.948
	C2	5.56	5.69	0.943
	C3	5.14	17.5	0.962
	C4	Not modeled *		
RSC700	C1	Not modeled		
	C2	Not modeled		
	C3	5.40	2.18	0.846
	C4	Not modeled		

* The quenching curve fitting was not performed because the detected fluorescence intensities of these components were too low and the fitting failed.

modeling results further confirmed that the C_L values of the four components of biochar DOM all decreased with the increasing pyrolysis temperature (Table 3). A similar trend was also found in our previous study of Cu complexion with JAS biochar DOM (Wei et al., 2019a). However, unlike the JAS biochar DOM having the carboxyl C contents of 13.4–25.2% and C_L values of 9.87–93.2 μmol L^{-1}, here the RSC biochar DOM only contained 8.9–11.3% carboxyl C, and lower C_L values of 2.18–17.7 μmol L^{-1}. Therefore, it could be expected that the RSC biochar DOM has a much lower potential for binding and then facilitating heavy metal transport than JAS biochar DOM.

The binding affinity (log K_M) values for C1–C4 ranged from 4.94 to 5.65 (Table 3), which were close to those found for anthropogenic biochar DOM (4.38–6.06) (Wei et al., 2019a), and natural soil (5.15–5.94), sediment (4.77–5.39) and freshwater DOM (4.37–5.44) (Hu et al., 2017; Wei et al., 2015; Xu et al., 2013). Specifically, the log K_M values for three humic-like components slightly increased with rising pyrolysis temperature, further indicating that changes occurred in DOM components during the pyrolysis process. Besides carboxyl and phenolic groups, aromatic structures have been proven to be involved in cation-π interaction, especially for the transition metal, and thus they also function as binding sites (Wei et al., 2019b). As the total aromatic-C species, including quinonic C=O and aromatic C=C, accounts for 29.5%–31.9% of the total C (Table 2), the Cu-π interaction is expected to occur in DOM from biochars, particularly high-temperature ones. This could be partially responsible for the increased log K_M values. It is also noticed that for the three humic-like components, both the log K_M values of C1 and C2 were higher than that of C3, while the C_L values of C1 and C2 were remarkably lower than that of C3. The opposite trends for the log K_M and C_L values could be due to the formation of multidentate complexes (Plaza et al., 2006), which needs further study.

3.5. Environmental implications

As summarized in Fig. 6, both the content and composition of biochar-derived DOM are dependent on pyrolysis temperature. With a rising temperature from 300 to 700 °C, the total amount of biochar released DOM decreased, and DOM was progressively transformed into a more stable form, comprising primarily of humic-like substance with high aromaticity. The Cu binding sequence was humic-like C3 > humic-like C2 > humic-like C1 > protein-like C4 at all temperatures, which suggests that the humic-like substances exhibited higher Cu binding affinities than the protein-like substance. Moreover, with the rising temperature, the Cu binding capacity also decreased significantly. All of these results strongly indicated that biochar produced at a lower temperature has a higher risk of Cu mobilization, and it is highly recommended to testify Cu binding characteristics of DOM before biochar use in the environment. Besides, this study also indicates that fluorescence quenching, together with PARAFAC and 2D-COS analysis, is a useful tool for a quick assessment of the potential co-migration risk of heavy metals with biochar DOM.

On the other hand, speciation is crucial to bioavailability and toxicity of heavy metals in soil ecosystems. Cu bioavailability could be reduced by DOM of large molecular weight (e.g., humic substances), but enhanced by DOM of small molecular weight (e.g., protein substances) (Philipps et al., 2018; Shi et al., 2017; Wang et al., 2010). If RSC biochar, particularly RSC500 and RSC700, is applied to Cu-contaminated soil, a relatively small amount of DOM would be released from the biochar. Meanwhile, based on the low binding capacity of the biochar DOM, Cu in soil could be primarily immobilized by the bulk biochar rather than being mobilized by its DOM. Further, the high humic-like fraction of biochar DOM would bind Cu in water and reduce its aquatic bioavailability. As a result, the environmental risk from RSC biochar DOM would be low. Cautions, however, should be taken for biochars that can release a large amount of DOM with high content of protein substance and good heavy metal binding capacity. Removal of its DOM before biochar use would be required.

4. Conclusions

With the increase of charring temperature, the aromaticity of biochar DOM increased, whereas the proportion of metal complex-

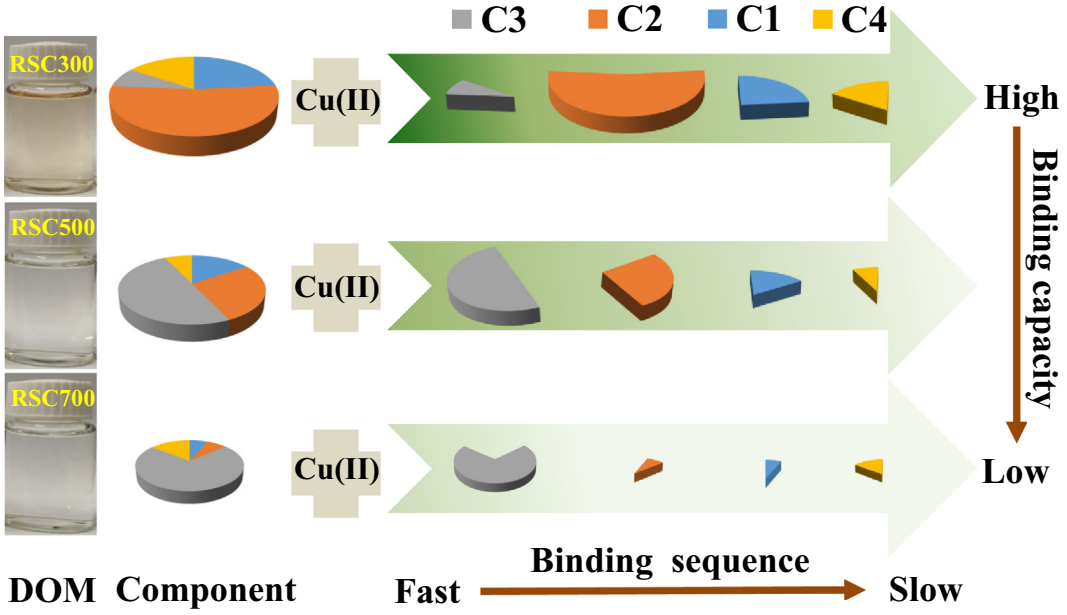

Fig. 6. Copper binding performance of DOM from biochars produced at different pyrolysis temperatures. Different colors of the pie represent different DOM components: humic-like C1, humic-like C2, humic-like C3, and protein-like C4. The size of the pie represents the total amount of DOM derived from biochar at different temperatures. The horizontal arrow represents the sequence of Cu binding affinity by different DOM components, and the vertical arrow represents the Cu binding capacity by biochar DOM produced at different temperatures.

ing sites (e.g., carboxyl and phenolic groups) decreased. The biochar DOM, regardless of pyrolysis temperature, was mostly composed of three types of humic-like components, and a small amount of a protein-like component. In reaction with Cu(II), the humic-like components responded faster than the protein-like component and showed a higher binding capacity and affinity. As pyrolysis temperature increased, both the total DOM content and its humic-like components remarkably decreased, resulting in a substantial reduction in Cu-binding capacity. The temperature-dependent molecular characteristics of biochar DOC, as well as its Cu binding properties, can be used to predict the behavior of DOM in biochar-amended systems and to help the selection of suitable biochars for specific environmental applications.

Declaration of Competing Interest

Authors declare that no conflict of interest exits in the submission of this manuscript (Limited Cu(II) binding to biochar DOM: Evidence from C K-edge NEXAFS and EEM-PARAFAC combined with two-dimensional correlation analysis).

Acknowledgments

This research was supported by the National Natural Science Foundation of China (41501522, 41671319, 41977139), the Yantai Key Research and Development Program (2019XDHZ104), the National Key Research and Development Program of China (2016YFD0200303, 2016YFE0106400), and the One Hundred Talents Program of Chinese Academy of Sciences (Y629041021).

Appendix A. Supplementary material

Supplementary data to this article can be found online at https://doi.org/10.1016/j.scitotenv.2019.134919.

References

Abdulla, H.A.N., Minor, E.C., Dias, R.F., Hatcher, P.G., 2010. Changes in the compound classes of dissolved organic matter along an estuarine transect: a study using FTIR and C-13 NMR. Geochim. Cosmochim. Acta 74 (13), 3815–3838.

Awad, Y.M., Ok, Y.S., Abrigata, J., Beiyuan, J., Beckers, F., Tsang, D.C.W., Rinklebe, J., 2018. Pine sawdust biomass and biochars at different pyrolysis temperatures change soil redox processes. Sci. Total Environ. 625, 147–154.

Baken, S., Degryse, F., Verheyen, L., Merckx, R., Smolders, E., 2011. Metal complexation properties of freshwater dissolved organic matter are explained by its aromaticity and by anthropogenic ligands. Environ. Sci. Technol. 45 (7), 2584–2590.

Beesley, L., Moreno-Jimenez, E., Gomez-Eyles, J.L., 2010. Effects of biochar and greenwaste compost amendments on mobility, bioavailability and toxicity of inorganic and organic contaminants in a multi-element polluted soil. Environ. Pollut. 158 (6), 2282–2287.

Chen, G.H., Zhang, Z.R., Zhang, Z.Y., Zhang, R.D., 2018. Redox-active reactions in denitrification provided by biochars pyrolyzed at different temperatures. Sci. Total Environ. 615, 1547–1556.

Chen, W., Habibul, N., Liu, X.Y., Sheng, G.P., Yu, H.Q., 2015. FTIR and synchronous fluorescence heterospectral two-dimensional correlation analyses on the binding characteristics of copper onto dissolved organic matter. Environ. Sci. Technol. 49 (4), 2052–2058.

Cole, D.P., Smith, E.A., Lee, Y.J., 2012. High-resolution mass spectrometric characterization of molecules on biochar from pyrolysis and gasification of switchgrass. Energ. Fuel 26 (6), 3803–3809.

Diffey, B.L., 2002. Sources and measurement of ultraviolet radiation. Methods 28 (1), 4–13.

Dong, X.L., Ma, L.Q., Gress, J., Harris, W., Li, Y.C., 2014. Enhanced Cr(VI) reduction and As(III) oxidation in ice phase: important role of dissolved organic matter from biochar. J. Hazard. Mater. 267, 62–70.

El-Naggar, A., El-Naggar, A.H., Shaheen, S.M., Sarkar, B., Chang, S.X., Tsang, D.C.W., Rinklebe, J., Ok, Y.S., 2019. Biochar composition-dependent impacts on soil nutrient release, carbon mineralization, and potential environmental risk: a review. J. Envrion. Manag. 241, 458–467.

Fellman, J.B., Hood, E., Spencer, R.G.M., 2010. Fluorescence spectroscopy opens new windows into dissolved organic matter dynamics in freshwater ecosystems: a review. Limnol. Oceanogr. 55 (6), 2452–2462.

Harvey, O.R., Herbert, B.E., Kuo, L.J., Louchouarn, P., 2012. Generalized two-dimensional perturbation correlation infrared spectroscopy reveals mechanisms for the development of surface charge and cecalcitrance in plant-derived biochars. Environ. Sci. Technol. 46 (19), 10641–10650.

Hu, B., Wang, P., Wang, C., Qian, J., Hou, J., Cui, X., Zhang, N., 2017. The effect of anthropogenic impoundment on dissolved organic matter characteristics and copper binding affinity: Insights from fluorescence spectroscopy. Chemosphere 188, 424–433.

Huang, M., Li, Z., Luo, N., Yang, R., Wen, J., Huang, B., Zeng, G., 2019. Application potential of biochar in environment: insight from degradation of biochar-derived DOM and complexation of DOM with heavy metals. Sci. Total Environ. 646, 220–228.

Hur, J., Lee, B.M., 2014. Characterization of copper binding properties of extracellular polymeric substances using a fluorescence quenching approach combining two-dimensional correlation spectroscopy. J. Mol. Struct. 1069, 79–84.

Ishii, S.K.L., Boyer, T.H., 2012. Behavior of reoccurring PARAFAC components in fluorescent dissolved organic matter in natural and engineered systems: a critical review. Environ. Sci. Technol. 46 (4), 2006–2017.

Kim, H.-B., Kim, S.-H., Jeon, E.-K., Kim, D.-H., Tsang, D.C.W., Alessi, D.S., Kwon, E.E., Baek, K., 2018. Effect of dissolved organic carbon from sludge, rice straw and spent coffee ground biochar on the mobility of arsenic in soil. Sci. Total Environ. 636, 1241–1248.

Kleber, M., Nico, P.S., Plante, A., Filley, T., Kramer, M., Swanston, C., Sollins, P., 2011. Old and stable soil organic matter is not necessarily chemically recalcitrant: implications for modeling concepts and temperature sensitivity. Global Change Biol. 17 (2), 1097–1107.

Kleen, M., Gellerstedt, G., 1995. Influence of inorganic species on the formation of polysaccharide and lignin degradation products in the analytical pyrolysis of pulps. J. Anal. Appl. Pyrolysis 35 (1), 15–41.

Kloss, S., Zehetner, F., Dellantonio, A., Hamid, R., Ottner, F., Liedtke, V., Schwanninger, M., Gerzabek, M.H., Soja, G., 2012. Characterization of slow pyrolysis biochars: effects of feedstocks and pyrolysis temperature on biochar properties. J. Environ. Qual. 41 (4), 990–1000.

Lakowicz, J.R., 2006. Principles of Fluorescence Spectroscopy, third ed., Springer, p. 278.

Lawaetz, A.J., Stedmon, C.A., 2009. Fluorescence intensity calibration using the Raman scatter peak of water. Appl. Spectrosc. 63 (8), 936–940.

Lee, M.-H., OK, Y.S., Hur, J., 2018. Dynamic variations in dissolved organic matter and the precursors of disinfection by-products leached from biochars: leaching experiments simulating intermittent rain events. Environ. Pollut. 242, 1912–1920.

Li, G., Khan, S., Ibrahim, M., Sun, T.R., Tang, J.F., Cotner, J.B., Xu, Y.Y., 2018. Biochars induced modification of dissolved organic matter (DOM) in soil and its impact on mobility and bioaccumulation of arsenic and cadmium. J. Hazard. Mater. 348, 100–108.

Li, M., Zhang, A.F., Wu, H.M., Liu, H., Lv, J.L., 2017. Predicting potential release of dissolved organic matter from biochars derived from agricultural residues using fluorescence and ultraviolet absorbance. J. Hazard. Mater. 334, 86–92.

Li, Z.C., Song, Z.L., Singh, B.P., Wang, H.L., 2019. The impact of crop residue biochars on silicon and nutrient cycles in croplands. Sci. Total Environ. 659, 673–680.

Lichtman, J.W., Conchello, J.A., 2005. Fluorescence microscopy. Nat. Methods 2 (12), 910–919.

Liu, C.H., Chu, W.Y., Li, H., Boyd, S.A., Teppen, B.J., Mao, J.D., Lehmann, J., Zhang, W., 2019. Quantification and characterization of dissolved organic carbon from biochars. Geoderma 335, 161–169.

Lomascolo, A., Uzan-Boukhris, E., Sigoillot, J.C., Fine, F., 2012. Rapeseed and sunflower meal: a review on biotechnology status and challenges. Appl. Microbiol. Technol. 95, 1105–1114.

Lu, J., Zhang, C., Wu, J., Luo, Y.M., 2017. Adsorptive removal of bisphenol A using N-doped biochar made of *Ulva prolifera*. Water Air Soil Pollut. 228, 327.

Luo, L., Lv, J.T., Chen, Z., Huang, R.X., Zhang, S.Z., 2017. Insights into the attenuated sorption of organic compounds on black carbon aged in soil. Environ. Pollut. 231, 1469–1476.

Luster, J., Lloyd, T., Sposito, G., Fry, I.V., 1996. Multi-wavelength molecular fluorescence spectrometry for quantitative characterization of copper(II) and aluminum(III) complexation by dissolved organic matter. Environ. Sci. Technol. 30 (5), 1565–1574.

Meng, F.D., Yuan, G.D., Wei, J., Bi, D.X., Wang, H.L., 2017. Leonardite-derived humic substances are great adsorbents for cadmium. Environ. Sci. Pollut. R. 24 (29), 23006–23014.

Ministry of Environmental Protection and the Ministry of Land and Resources of the People's Republic of China (MEP and MLR), 2014. Bulletin on national survey of soil contamination (2014). China Environmental Protection Industry, Beijing (10–11 pp. in Chinese).

Noda, I., Ozaki, Y., 2004. Two-Dimensional Correlation Spectroscopy: Applications in Vibrational and Optical Spectroscopy. John Wiley & Sons.

Philipps, R.R., Xu, X., Mills, G.L., Bringolf, R.B., 2018. Impact of natural organic matter and increased water hardness on DGT prediction of copper bioaccumulation by yellow lampmussel (*Lampsilis cariosa*) and fathead minnow (*Pimephales promelas*). Environ. Pollut. 241, 451–458.

Plaza, C., Brunetti, G., Senesi, N., Polo, A., 2006. Molecular and quantitative analysis of metal ion binding to humic acids from sewage sludge and sludge-amended soils by fluorescence spectroscopy. Environ. Sci. Technol. 40 (3), 917–923.

Qi, L., Xie, H., Gagné, J.P., Chaillou, G., Massicotte, P., Yang, G.P., 2018. Photoreactivities of two distinct dissolved organic matter pools in groundwater of a subarctic island. Mar Chem. 202, 97–120.
Qu, X.L., Fu, H.Y., Mao, J.D., Ran, Y., Zhang, D.N., Zhu, D.Q., 2016. Chemical and structural properties of dissolved black carbon released from biochars. Carbon 96, 759–767.
Rajapaksha, A.U., Ok, Y.S., El-Naggar, A., Kim, H., Song, F., Kang, S., Tsang, Y.F., 2019. Dissolved organic matter characterization of biochars produced from different feedstock materials. J. Environ. Manage. 233, 393–399.
Schafer, T., Buckau, G., Artinger, R., Kim, J.I., Geyer, S., Wolf, M., Bleam, W.F., Wirick, S., Jacobsen, C., 2005. Origin and mobility of fulvic acids in the Gorleben aquifer system: implications from isotopic data and carbon/sulfur XANES. Org. Geochem. 36 (4), 567–582.
Sullivan, A.L., Ball, R., 2012. Thermal decomposition and combustion chemistry of cellulosic biomass. Atmos. Environ. 47 (1), 133–141.
Shi, W., Jin, Z.F., Hu, S.Y., Fang, X.M., Li, F.L., 2017. Dissolved organic matter affects the bioaccumulation of copper and lead in *Chlorella pyrenoidosa*: a case of long-term exposure. Chemosphere 174, 447–455.
Singh, B., Fang, Y.Y., Cowie, B.C.C., Thomsen, L., 2014. NEXAFS and XPS characterisation of carbon functional groups of fresh and aged biochars. Org. Geochem. 77, 1–10.
Smith, C.R., Hatcher, P.G., Kumar, S., Lee, J.W., 2016. Investigation into the sources of biochar water-soluble organic compounds and their potential toxicity on aquatic microorganisms. ACS Sustain. Chem. Eng. 4 (5), 2550–2558.
Sun, Y.Q., Yu, I.K.M., Tsang, D.C.W., Cao, X.D., Lin, D.H., Wang, L.L., Graham, N.J.D., Alessi, D.S., Komárek, M., Ok, Y.S., Feng, Y.J., Li, X.D., 2019. Multifunctional iron-biochar composites for the removal of potentially toxic elements, inherent cations, and hetero-chloride from hydraulic fracturing wastewater. Environ. Int. 124, 521–532.
Thyrel, M., Backman, R., Thånell, K., Karunakaran, C., Skyllberg, U., Lestander, T.A., 2016. Nanomapping and speciation of C and Ca in thermally treated lignocellulosic cell walls using scanning transmission X-ray microscopy and K-edge XANES. Fuel 167, 149–157.
Tu, C., Liu, Y., Wei, J., Li, L.Z., Scheckel, K.G., Luo, Y.M., 2018. Characterization and mechanism of copper biosorption by a highly copper-resistant fungal strain isolated from copper-polluted acidic orchard soil. Environ. Sci. Pollut. Res. 25 (25), 24965–24974.
Uchimiya, M., Lima, I.M., Klasson, K.T., Wartelle, L.H., 2010. Contaminant immobilization and nutrient release by biochar soil amendment: roles of natural organic matter. Chemosphere 80 (8), 935–940.
Uchimiya, M., Ohno, T., He, Z.Q., 2013. Pyrolysis temperature-dependent release of dissolved organic carbon from plant, manure, and biorefinery wastes. J. Anal. Appl. Pyrolysis 104, 84–94.
Wang, X., Chen, X., Liu, S., Ge, X., 2010. Effect of molecular weight of dissolved organic matter on toxicity and bioavailability of copper to lettuce. J. Environ. Sci. (China) 22 (12), 1960–1965.
Wei, J., Han, L., Song, J., Chen, M.F., 2015. Evaluation of the interactions between water extractable soil organic matter and metal cations (Cu(II), Eu(III)) using Excitation-Emission matrix combined with parallel factor analysis. Int. J. Mol. Sci. 16 (7), 14464–14476.
Wei, J., Tu, C., Yuan, G.D., Bi, D.X., Wang, H.L., Zhang, L.J., Theng, B.K.G., 2019a. Pyrolysis temperature-dependent changes in the characteristics of biochar-borne dissolved organic matter and its copper binding properties. Bull. Environ. Contam. Toxicol. 103, 169–174.
Wei, J., Tu, C., Yuan, G.D., Liu, Y., Bi, D.X., Xiao, L., Lu, J., Theng, B.K.G., Wang, H.L., Zhang, L.J., Zhang, X.Z., 2019b. Assessing the effect of pyrolysis temperature on the molecular properties and copper sorption capacity of a halophyte biochar. Environ. Pollut. 251, 56–65.
Wu, H.M., Dong, X.Y., Liu, H., 2018a. Evaluating fluorescent dissolved organic matter released from wetland-plant derived biochar: effects of extracting solutions. Chemosphere 212, 638–644.
Wu, H.M., Qi, Y.S., Dong, L., Zhao, X., Liu, H., 2019a. Revealing the impact of pyrolysis temperature on dissolved organic matter released from the biochar prepared from *Typha orientalis*. Chemosphere 228, 264–270.
Wu, J., Ye, J., Peng, H., Wu, M., Shi, W., Liang, Y., Liu, W., 2018b. Solar photolysis of soluble microbial products as precursors of disinfection by-products in surface water. Chemosphere 201, 66–76.
Wu, P., Ata-Ul-Karim, S.T., Singh, B.P., Wang, H.L., Wu, T.L., Liu, C., Fang, G.D., Zhou, D.M., Wang, Y.J., Chen, W.F., 2019b. A scientometric review of biochar research in the past 20 years (1998–2018). Biochar 1 (1), 23–43.
Xia, S.P., Song, Z.L., Jeyakumar, P., Shaheen, S.M., Rinklebe, J., Ok, Y.S., Bolan, N., Wang, H. L., 2019. A critical review on bioremediation technologies for Cr(VI)-contaminated soils and wastewater. Crit. Rev. Environ. Sci. Technol. 49, 1027–1078.
Xiao, X., Chen, B.L., Zhu, L.Z., 2014. Transformation, morphology, and dissolution of silicon and carbon in rice straw-derived biochars under different pyrolytic temperatures. Environ. Sci. Technol. 48 (6), 3411–3419.
Xu, H., Yu, G., Yang, L., Jiang, H., 2013. Combination of two-dimensional correlation spectroscopy and parallel factor analysis to characterize the binding of heavy metals with DOM in lake sediments. J. Hazard. Mater. 263 (Pt 2), 412–421.
Xu, X.Y., Huang, D.X., Zhao, L., Kan, Y., Cao, X.D., 2016. Role of inherent inorganic constituents in SO_2 sorption ability of biochars derived from three biomass wastes. Environ. Sci. Technol. 50 (23), 12957–12965.
Yang, H.P., Yan, R., Chen, H.P., Lee, D.H., Zheng, C.G., 2007. Characteristics of hemicellulose, cellulose and lignin pyrolysis. Fuel 86 (12–13), 1781–1788.
Yang, X., Tsibart, A., Nam, H., Hur, J., El-Naggar, A., Tack, F.M., Wang, C.H., Lee, Y.H., Tsang, D.C., Ok, Y.S., 2019. Effect of gasification biochar application on soil quality: trace metal behavior, microbial community, and soil dissolved organic matter. J. Hazard. Mater. 365, 684–694.
Zhou, Y.Q., Yao, X.L., Zhang, Y.B., Shi, K., Zhang, Y.L., Jeppesen, E., Gao, G., Zhu, G.W., Qin, B.Q., 2017. Potential rainfall-intensity and pH-driven shifts in the apparent fluorescent composition of dissolved organic matter in rainwater. Environ. Pollut. 224, 638–648.